Preparation and Solid-State Characterization of Dapsone Drug–Drug Co-Crystals

ARTICLE *in* CRYSTAL GROWTH & DESIGN · AUGUST 2014

Impact Factor: 4.89 · DOI: 10.1021/cg500668a

CRYSTAL GROWTH & DESIGN

Article

pubs.acs.org/crystal

Preparation and Solid-State Characterization of Dapsone Drug–Drug Co-Crystals

Linglei Jiang, Ying Huang, Qi Zhang, Hongyan He, Yun Xu, and Xuefeng Mei*

Pharmaceutical Analytical & Solid-State Chemistry Research Center, Shanghai Institute of Materia Medica, Chinese Academy of Sciences, Shanghai 201203, China

Supporting Information

ABSTRACT: Pharmaceutical co-crystals involving two active pharmaceutical ingredients are rarely revealed in the literature. In this work, crystal engineering principles were exercised to guide the design and synthesis of the Biopharmaceutics Classification System class IV drug dapsone (DAP). We reported six drug–drug co-crystals of DAP with sulfanilamide, flavone, luteolin, caffeine in 1:1 stoichiometry, caffeine in 1:2 stoichiometry, and 2(3*H*)-benzothiazolone. Bioactive coformers were deliberately selected. The resulting co-crystals were fully characterized by a range of analytical technologies, including X-ray powder diffraction, Fourier transform infrared spectroscopy, polarized light microscopy, differential scanning calorimetry, and thermogravimetric analysis, etc. Single-crystal structure analysis reveals that reoccurring supramolecular synthons are observed in different DAP co-crystals. Equilibrium solubility and intrinsic dissolution rates were also compared with those of the parent drug. This work expands the pharmaceutically acceptable solid forms of DAP and supplements the successful cases of drug–drug co-crystals.

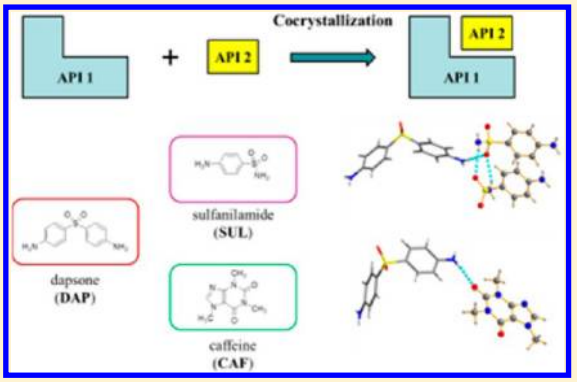

INTRODUCTION

Dapsone (DAP) was originally introduced as a sulfur-containing compound for antibacterial investigation in 1936, and the drug was studied for the treatment of a totally different array of diseases during subsequent decades.[1] Currently, it is employed to treat tuberculosis, leprosy, malaria, Kaposi's sarcoma, dermatoses, and AIDS-related pneumonia.[1−4] The story of reinvention of DAP in the clinic has aroused general interest in drug development history. DAP is classified as a class IV compound according to the Biopharmaceutics Classification System (BCS) in the literature.[5,6] The drug is commercially available as an oral tablet and a topical gel. It is slowly absorbed with 70−80% bioavailability in an acidic environment.[7] Despite its therapeutic potential, the low solubility (0.16 mg/mL in water) was found to result in a low therapeutic index and high microbial resistance.[8−10] To overcome the solubility limitation, several entities such as amino acid derivatives, inclusion compounds with β-cyclodextrin, and nanoemulsion formulations have been developed.[8,9,11] In addition, co-crystals of DAP with 3,5-dinitrobenzoic acid, 1,3,5-trinitrobenzene, 5-nitroisophthalic acid, ε-caprolactam, and 4,4-bipyridine were also reported.[3,4,12,13] Although different DAP co-crystals were synthesized, none of the coformers are pharmaceutically acceptable and hence cannot be applied directly in the drug development.

Over the past decade, pharmaceutical co-crystal screening has rapidly developed into a general method for modifying drugs' physicochemical properties, including the solubility, dissolution rate, stability toward thermal and humid stress, and compressibility aspects.[14−29] As a subset of co-crystals, drug–drug co-crystals may not only lead to the modification of the physicochemical properties, but also present new opportunities for the development of combinational therapies. Drug–drug co-crystals fulfill the criteria for patent eligibility: novelty, utility, and nonobviousness.[30] Consequently, there has been a growing interest in the study of drug–drug co-crystals reflected in the increasing number of publications and patent applications in recent years.[31−36]

The pure dapsone drug can exist as an anhydrate, in hydrated form, and in three solvated forms, including dichloromethane, 1,4-dioxane, and tetrahydrofuran solvates. Crystal structures of the anhydrate and the stable hydrate forms are reported.[3,37,38] On the basis of a close analysis of all the related single-crystal data of DAP available in the literature, intermolecular hydrogen bonds between the aromatic amino groups and the oxygen atoms of the sulfonyl moieties via synthon **I** (N−H···O═S) are frequently observed in the structures (Figure 1). As the structure of DAP contains two aromatic amino groups, we envisioned that any compound containing sulfonyl groups could potentially form additional H-bonding with the unsatisfied amino groups of DAP molecules. Furthermore, similar H-bonding interactions between aromatic amino groups

Received: May 7, 2014
Revised: July 25, 2014
Published: August 1, 2014

   dx.doi.org/10.1021/cg500668a | *Cryst. Growth Des.* 2014, 14, 4562−4573

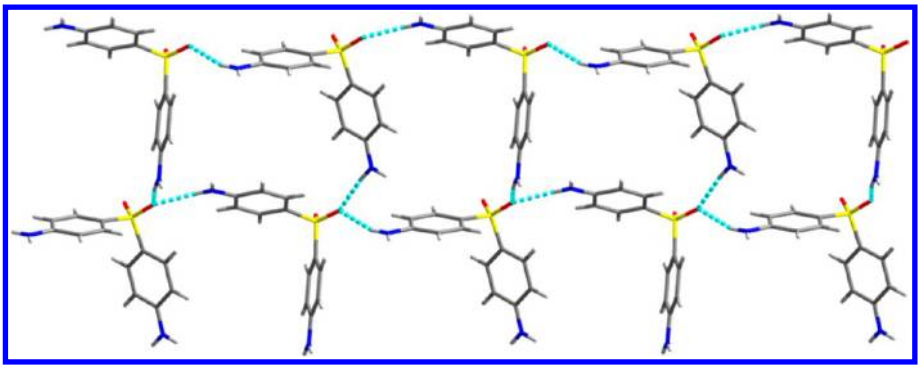

Figure 1. Hydrogen-bonding interactions observed in the DAP hydrate form.

Table 1. CSD Statistics of Possible Supramolecular Synthons in DAP with Aromatic Amine Functionalities

No.	Synthon	Hits	Survey Constrains
I	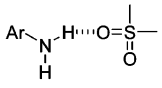	262	Intermolecular shorter than sum of VdW radii + 0.0 $R_{factor} \leqslant 0.05$ No disordered No errors No ions
II	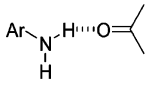	376	

Scheme 1. Chemical Structures of DAP and Potential Coformers[a]

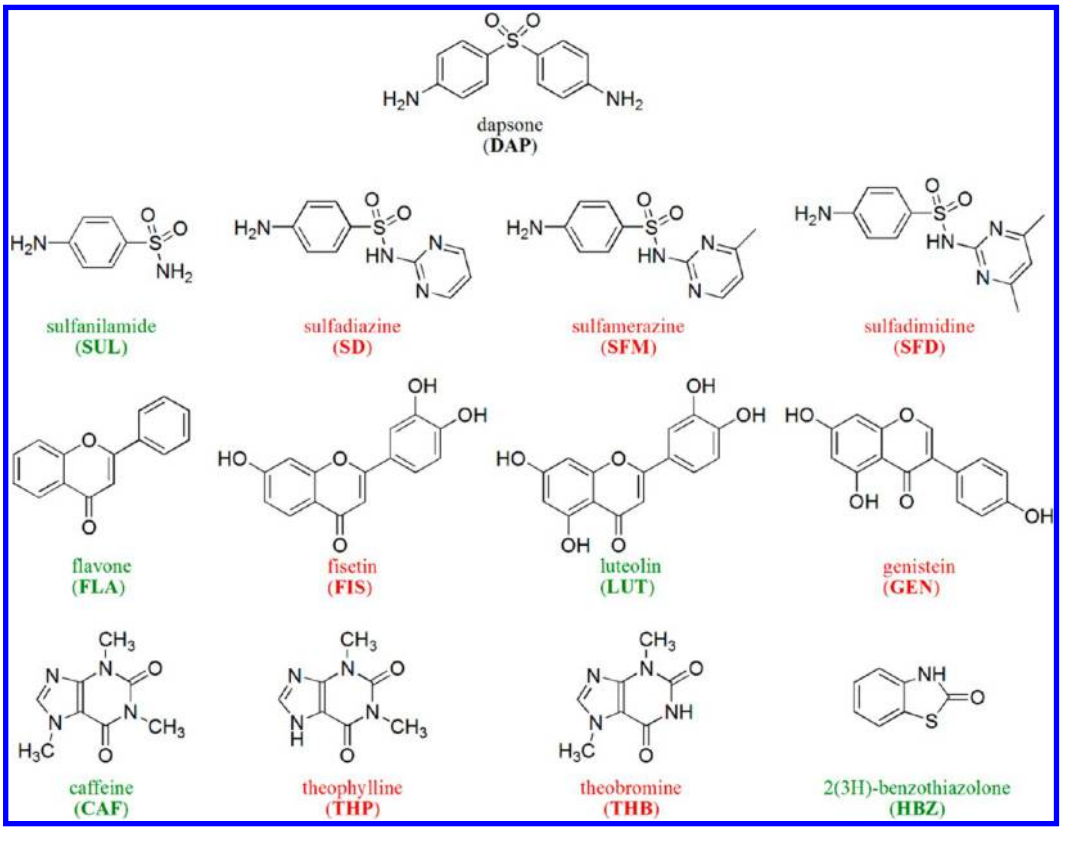

[a]Successful selected coformers are labeled in green, and unsuccessful ones are labeled in red.

dx.doi.org/10.1021/cg500668a | *Cryst. Growth Des.* 2014, 14, 4562−4573

and carbonyl moieties, as depicted in synthon **II** (N−H···O=C), could also be utilized as an alternative to the sulfonyl groups in designing DAP co-crystals. A survey of the two synthons in the Cambridge Structural Database (CSD) was performed (CSD version 5.35, February 2014). Separate searches were done for synthons **I** and **II**. There are 2031 structures containing primary aromatic amino groups. Out of those entries, 262 (12.9%) hits form synthon **I**, suggesting that the aromatic amino group is likely to form supramolecular interactions with sulfonyl groups. There are 376 (18.5%) hits containing synthon **II**, which implies that the interaction between the aromatic amino group and carbonyl groups is also frequent (Table 1). On the basis of the synthon design approach, a series of bioactive compounds with either sulfonyl or carbonyl moieties were selected as coformers (Scheme 1). Interestingly, co-crystallization screening experiments resulted in six successful co-crystals with single-crystal structures solved.

Unlike the previously reported DAP co-crystals, in this work, six DAP co-crystals were synthesized with biologically active ingredients as coformers. Sulfanilamide is a chemical analogue of DAP and exhibits potent antibacterial activity by a mechanism similar to that of DAP.[39] Flavonoids are generally recognized as active pharmaceutical ingredients with health-prolonging effects attributed to their antibacterial, antioxidant, antitumor, and anti-inflammatory properties.[40−42] Caffeine and its xanthine analogues theophylline and theobromine have been approved by the FDA as "generally regarded as safe" (GRAS) agents that also have activity as anti-inflammatories and lipolytics.[43] Hence, the development of dapsone−sulfa drug, dapsone−flavonoid, and dapsone−caffeine drug−drug co-crystals may open the field for antibacterial combination, and they also possess the potential to be novel antioxidants and anti-inflammatory drugs. 2-Hydroxybenzothizole is well documented to have anticonvulsant activity, and a large chemical series containing 2(3*H*)-benzothiazolinone moieties has been described for interactions with a number of molecular targets such as membrane and nuclear receptors.[44−46] The dapsone−2(3*H*)-benzothiazolinone co-crystal may find applications toward developing combinational anticonvulsant drugs. In this study, the single-crystal structures of all six co-crystals were revealed. The physicochemical properties were fully investigated by X-ray powder diffraction (XRPD), Fourier transform infrared (FT-IR) spectroscopy, polarized light microscopy (PLM), differential scanning calorimetry (DSC), and thermogravimetric analysis (TGA). Equilibrium solubility and intrinsic dissolution rates were compared with those of the parent drug as well. This work is the first to report co-crystals of DAP with pharmaceutically acceptable compounds and supplements the successful examples of the design and synthesis of drug−drug co-crystals.

EXPERIMENTAL SECTION

Materials. DAP was purchased from Shanghai Demo Biological Technological Co. Ltd. Sulfanilamide (SUL), sulfadiazine (SD), and 2(3*H*)-benzothiazolone (HBZ) were purchased from J&K Co. Ltd. Fisetin (FIS), luteolin (LUT), caffeine (CAF), theophylline (THP), and theobromine (THB) were purchased from Aladdin Co. Ltd. Sulfamerazine (SFM) and flavone (FLA) were purchased from Alfa Aesar Co. Ltd. Sulfadimidine (SFD) and genistein (GEN) were purchased from TCI Shanghai Co. Ltd. with greater than 99% purity. All analytical grade solvents were purchased from Sinopharm Chemical Reagent Co. and used without further purification. XRPD analysis of the commercially available DAP confirmed that it is in the anhydrous form (CSD ref code DAPSUO10).[37]

Preparation of Co-Crystals. Slow-evaporative crystallization experiments were carried out by dissolving each component in 2 mL of solvent according to Table 2. Crystals suitable for physicochemical characterization were harvested after slow evaporation of the corresponding solvent in a desiccator. Particularly, single crystals of DAP·SUL and DAP·FLA were obtained after 5 days of allowing the solvent to evaporate slowly. Single crystals of DAP·CAF-1 and DAP·HBZ were harvested after 1 day. However, it took about 1 month to obtain single crystals of DAP·LUT with good quality.

Table 2. Summary of Components in the Crystallization Experiments

co-crystal	API[a] amt (mg, mmol)	coformer amt (mg, mmol)	solvent
DAP·SUL	24.8, 0.1	34.4, 0.2	ethanol−acetone (v/v, 1/1)
DAP·FLA	24.8, 0.1	22.2, 0.1	ethanol−acetone (v/v, 1/1)
DAP·LUT	24.8, 0.1	28.6, 0.1	ethanol−acetone (v/v, 1/1)
DAP·CAF-1	24.8, 0.1	19.4, 0.1	ethyl acetate
DAP·CAF-2	24.8, 0.1	19.4, 0.1	ethyl acetate−methanol (v/v, 1/1)
DAP·HBZ	24.8, 0.1	15.1, 0.1	ethanol−acetone (v/v, 1/1)

[a]Active pharmaceutical ingredient.

Thermogravimetric Analysis. TGA was carried out on a Netzsch TG209 F3 instrument using N_2 as dry air with a flow rate of 20 mL/min and a scan rate of 10 °C/min.

Differential Scanning Calorimetry. DSC was performed with a PerkinElmer DSC 8500 instrument. Samples weighing 3−5 mg were heated in standard aluminum pans at scan rates from 10 to 200 °C/min under a nitrogen gas flow of 20 mL/min. Two-point calibration using indium and tin was carried out to check the temperature axis and heat flow of the equipment.

Single-Crystal X-ray Diffraction. Single-crystal X-ray diffraction (SCXRD) measurements were conducted on a Bruker Smart Apex II diffractometer using Mo Kα radiation (λ = 0.71073 Å) with a graphite monochromator. Integration and scaling of intensity data were accomplished using the SAINT program. The structures were solved by direct methods using SHELXS97, and refinement was carried out with the full-matrix least-squares technique using SHELXL97.[47]The hydrogen atoms were refined isotropically, and the heavy atoms were refined anisotropically. N−H and O−H hydrogens were located from difference electron density maps, and C−H hydrogens were placed in calculated positions and refined with a riding model. The data were corrected for the effects of absorption using SADABS. Crystallographic data in CIF format have been deposited at the Cambridge Crystallographic Data Center, CCDC Nos. 995302, 995303, 995304, 995306, and 995307 for DAP·SUL, DAP·FLA, DAP·LUT, DAP·CAF-1, DAP·CAF-2, and DAP·HBZ, respectively. The crystallographic data and refinement details are summarized in Table 3.

X-ray Powder Diffraction. XRPD was measured on a Bruker D8-ADVANCE X-ray diffractometer using a Cu Kα radiation (λ = 1.5418 Å). The voltage and current were 40 kV and 40 mA, respectively. Samples were measured in reflection mode in the 2θ range of 3−40° with a scan speed of 15 deg/min (step size 0.025°, step time 0.1 s) using a LynxEye detector. All data were acquired at ambient temperature (25 °C). The data were imaged and integrated with RINT Rapid and peak-analyzed with Origin 8.1 software. Calibration of the instrument was performed using the Corindon (Bruker AXS Korundprobe) standard.

Polarized Light Microscopy. All PLM examinations were performed on an XPV-400E polarizing microscope and an XPH-300 hot stage coupled with a JVC TK-C9201 EC digital video recorder (Shanghai Changfang Optical Instrument Co. Ltd.). Selective PLM photos for DAP co-crystals are presented in Figure 2.

dx.doi.org/10.1021/cg500668a | *Cryst. Growth Des.* 2014, 14, 4562−4573

Table 3. Crystallographic Data for the Co-Crystals

	DAP·SUL	DAP·FLA	DAP·LUT	DAP·CAF-1	DAP·CAF-2	DAP·HBZ
formula	$C_{12}H_{12}N_2O_2S$, $2(C_6H_8N_2O_2S)$	$C_{12}H_{12}N_2O_2S$, $C_{15}H_{10}O_2$	$C_{12}H_{12}N_2O_2S$, $C_{15}H_{10}O_6$, C_2H_6O	$C_{12}H_{12}N_2O_2S$, $C_8H_{10}N_4O_2$	$C_{12}H_{12}N_2O_2S$, $2(C_8H_{10}N_4O_2)$	$C_{12}H_{12}N_2O_2S$, C_7H_5NOS
cryst syst	monoclinic	monoclinic	monoclinic	orthorhombic	orthorhombic	monoclinic
space group	$C2/c$	$P2_1/n$	$P2_1/c$	$Pbca$	$Pna2_1$	$P2_1/n$
temp (K)	296(2)	296(2)	296(2)	296(2)	296(2)	296(2)
a (Å)	13.2304(2)	11.408(2)	22.293(2)	8.5613(6)	17.231(7)	5.8452(4)
b (Å)	30.2578(5)	11.644(3)	7.7975(7)	15.6676(9)	16.772(7)	14.3835(9)
c (Å)	13.6910(3)	18.448(4)	16.0553(14)	32.2872(19)	20.727(8)	21.7712(13)
α (deg)	90	90	90	90	90	90
β (deg)	102.448(1)	101.324(14)	91.814(5)	90	90	92.205(3)
γ (deg)	90	90	90	90	90	90
cell vol (Å^3)	5351.98(17)	2402.7(9)	2789.5(4)	4330.8(5)	5990(4)	1829.1(2)
calcd density (g/cm^3)	1.471	1.301	1.383	1.357	1.412	1.451
Z	8	4	4	8	8	4
no. of independent reflns	4283	2600	2744	3520	7135	3657
S	0.944	0.935	0.964	1.212	0.969	1.262
R_1	0.0405	0.0404	0.0694	0.0588	0.0724	0.0343
R_{int}	0.0272	0.0311	0.0922	0.0290	0.0801	0.0188
R_w	0.1448	0.1461	0.2169	0.1923	0.2028	0.1477

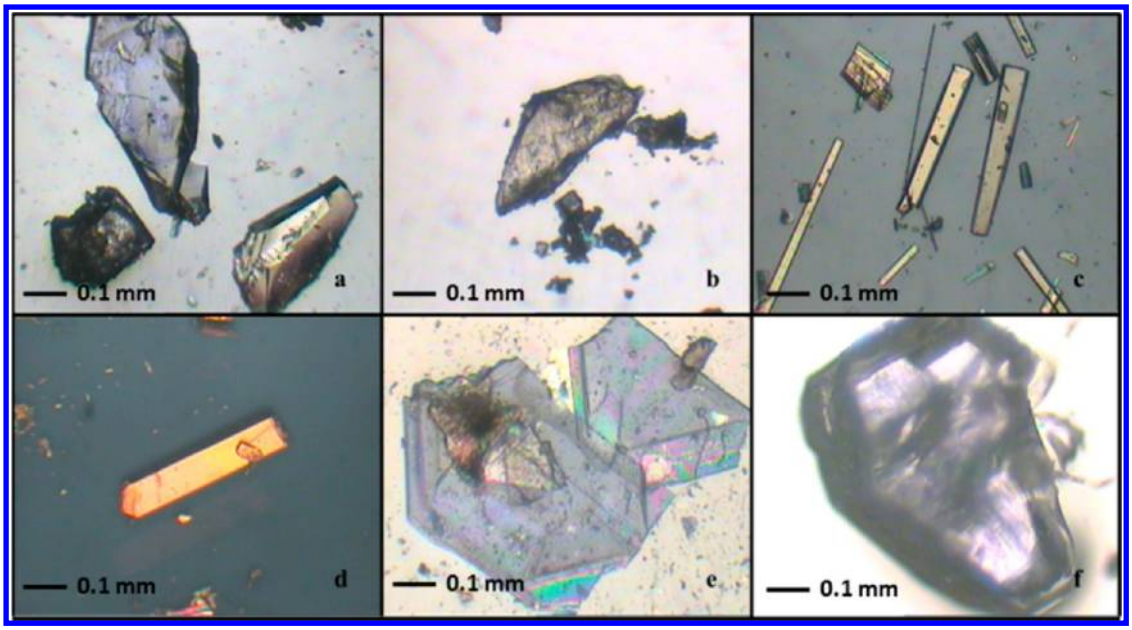

Figure 2. PLM photographs of DAP co-crystals: (a) DAP·SUL, (b) DAP·FLA, (c) DAP·LUT, (d) DAP·CAF-1, (e) DAP·CAF-2, (f) DAP·HBZ.

Fourier Transform Infrared Spectroscopy. FT-IR spectra were collected with a Nicolet-Magna FT-IR 750 spectrometer in the range from 4000 to 350 cm^{-1} with a resolution of 4 cm^{-1} at ambient conditions.

Solubility and Dissolution Experiments. Equilibrium solubility was determined by suspending an excess amount of each sample in 1.5 mL of distilled water (with 1% Tween 80), pH 2.0 glycine–hydrochloric acid buffer, pH 4.6 NaH_2PO_4–citric acid buffer, and pH 6.8 NaH_2PO_4–citric acid buffer at 37 °C in a Dragon LAB MS-H-Pro+ magnetic stirrer for 24 h. Upon equilibration, the solutions were filtered through 0.45 μm syringe filters, and the concentrations of the solutions were determined using an Agilent 1260 series Infinite HPLC instrument. In all the experiments, the HPLC instrument was equipped with a ZORBAX ECLIPSE-C18 column (4.6 × 150 mm, 5 μm). An injection volume of 10 μL was used with an eluent flow rate of 1 mL/min. The detection wavelength in the UV–vis range was set at 270 nm. The samples were gradient eluted with a mobile phase containing a mixture of acetonitrile and 15 mmol/L K_2HPO_4–H_3PO_4 pH 6.0 buffer. Typically, the gradient started at 5% acetonitrile and 95% K_2HPO_4–H_3PO_4 pH 6.0 buffer, which was maintained for 2 min, and was changed to 50% acetonitrile and 50% K_2HPO_4–H_3PO_4 pH 6.0 buffer in the following 9 min, which was maintained for 6 min. After each gradient analysis, the columns were re-equilibrated with the initial mobile phase (i.e., 5% acetonitrile). The observed retention time points for DAP, SUL, CAF, LUT, FLA, and HBZ are 9.7, 3.4, 7.2, 10.9, 16.0, and 10.9 min, respectively. No overlap between peaks for DAP or any coformers was observed. Intrinsic dissolution rate (IDR) experiments were conducted using a Mini-Bath dissolution apparatus equipped with a Julabo ED-5 heater/circulator. In each experiment, approximately 3 mg of sample was compressed into a 0.07 cm^2 disk in a rotating disk intrinsic dissolution die using a Mini-IDR press at a pressure of 40 bar for 1 min. Only one side of the disk was exposed to the dissolution medium. The intrinsic attachment was placed in a jar of 15 mL of distilled water containing 1% Tween 80 preheated at 37 °C

dx.doi.org/10.1021/cg500668a | Cryst. Growth Des. 2014, 14, 4562–4573

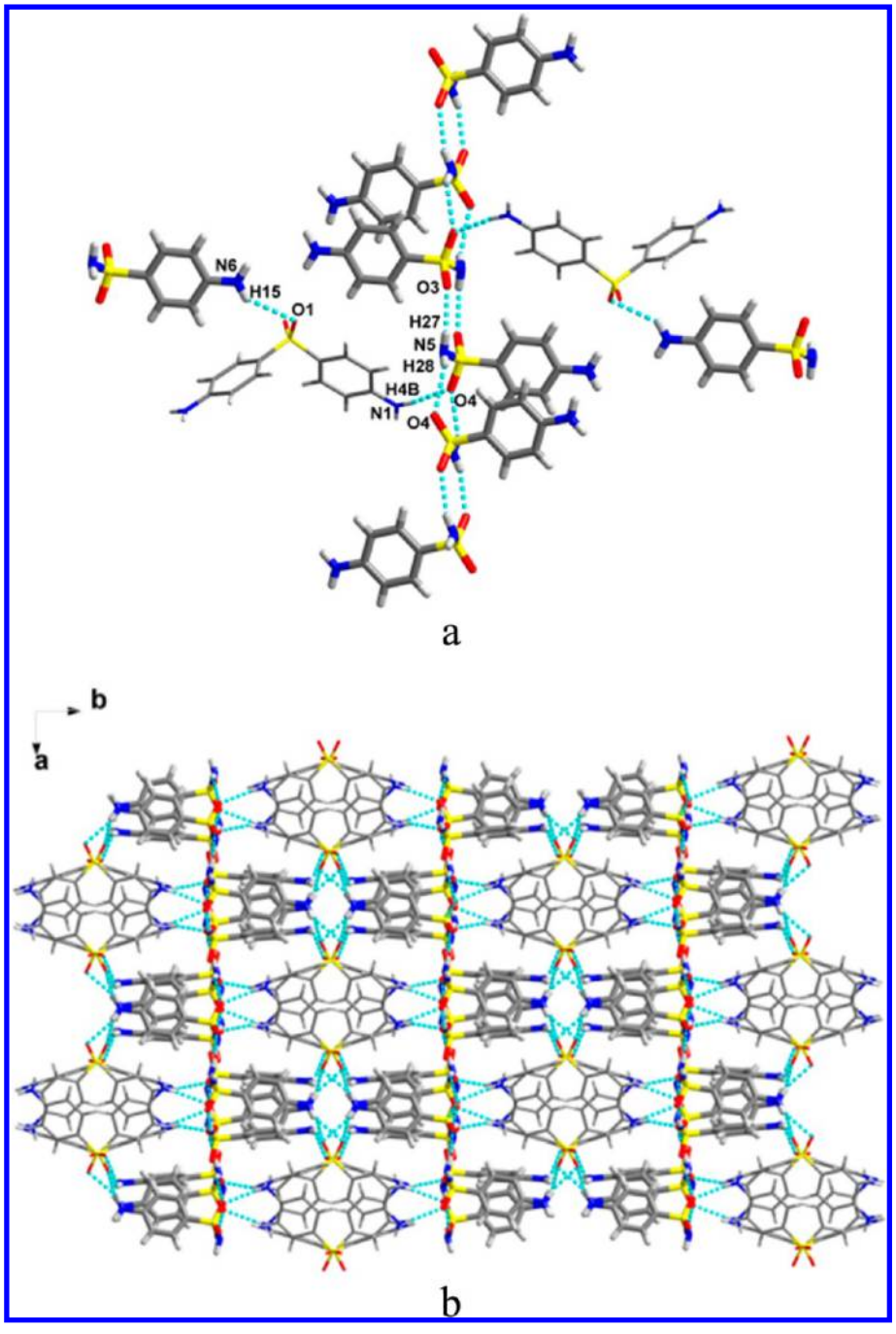

Figure 3. (a) Major hydrogen-bonding interactions and (b) 3D architecture of DAP·SUL.

and stirred at 75 rpm. At regular time intervals, 200 μL of the sample was withdrawn manually. The collected samples were diluted and assayed for DAP concentration using the HPLC method described above.

RESULTS AND DISCUSSION

Single-Crystal Structure Analysis. The dapsone molecule possesses a considerable potential for intermolecular interactions with coformer molecules via $-NH_2$ and $-SO_2-$ functional groups. Our strategy is to use these two important functional groups as interaction sites in the design and synthesis of multicomponent DAP co-crystals. It should be noted that the sulfonyl group is an ideal H-bonding acceptor to form H-bonding interactions with amino groups (Table 1). Intramolecular H-bonding interactions between the sulfonyl and amino groups of DAP (synthon **I**) would be expected in all the structures. However, by analyzing the single-crystal structures of DAP, we found that only part of the amino hydrogen atoms and sulfonyl oxygen atoms participated in the H-bonding formation. We envisioned that if other appropriate H-bonding donor/acceptor moieties are present, the hydrogen-bonding formation capability for the amino group and sulfonyl groups could be more satisfied. This opens new opportunities to accommodate additional H-bonding guest molecules, such as sulfamide, flavonoids, and alkaloids. A variety of coformers were selected for a co-crystallization screening experiment. Preferences were given to those coformers that have potential to form H-bonding interactions with amino moieties (Scheme 1). Out

dx.doi.org/10.1021/cg500668a | *Cryst. Growth Des.* 2014, 14, 4562−4573

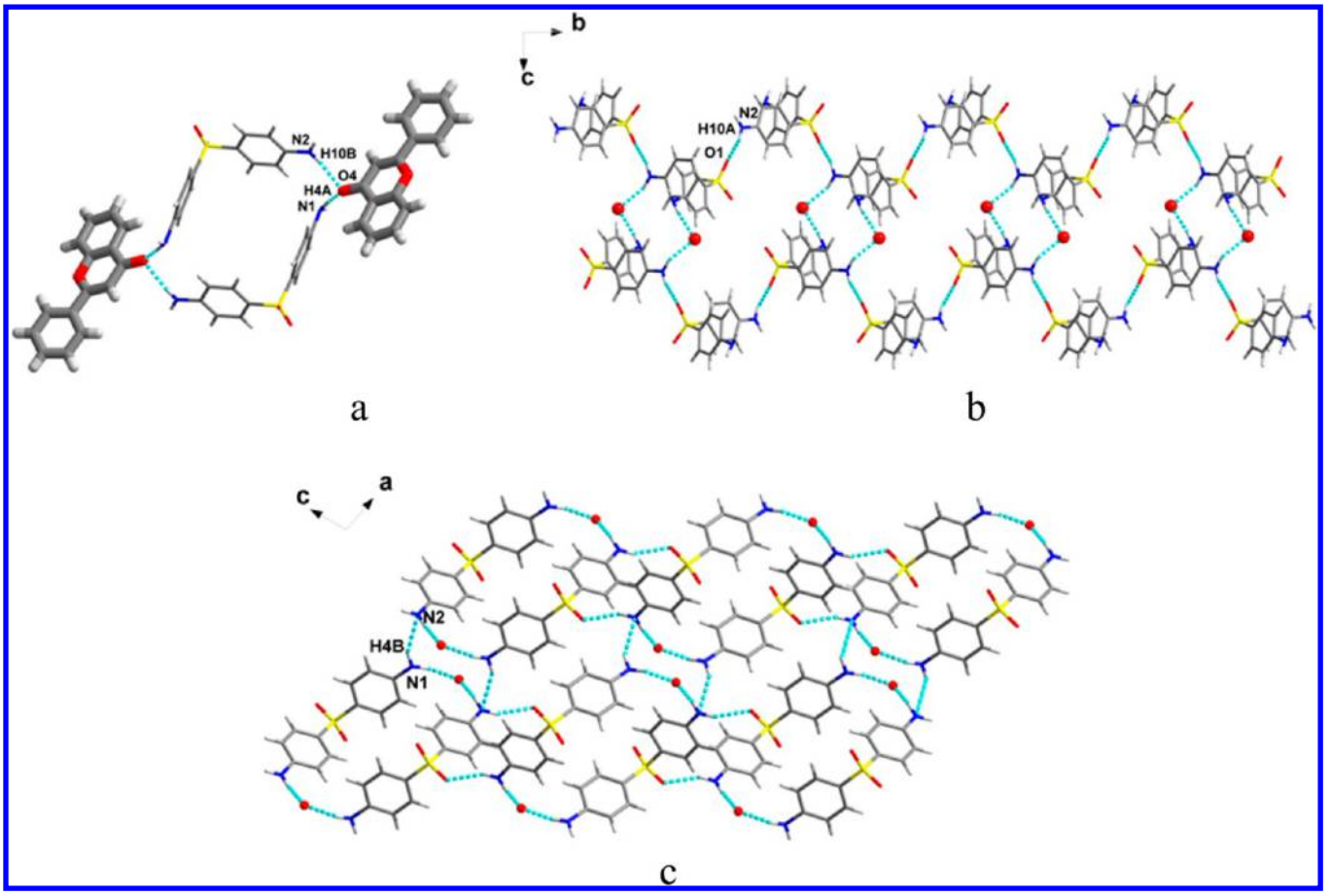

Figure 4. (a) Tetramer unit constructed by DAP and FLA. (b) 2D structure view along the *a* axis pf DAP·FLA. (c) Sheet structure along the *b* axis of DAP·FLA. Only the carbonyl oxygen atoms in FLA are depicted for clarity in (b) and (c).

of 12 potential coformers, 5 of them were found to form co-crystals with DAP. The crystallographic data for co-crystals are summarized in Table 3, and the hydrogen bond information is listed in Table S1 (Supporting Information).

DAP·SUL (1:2) Co-Crystal. As a structural analogue to DAP, sulfanilamide contains both sulfonamide and aromatic amino functionalities. The DAP·SUL co-crystal was designed on the basis of the analogue−analogue co-crystal formation principle. DAP and SUL were crystallized in 1:2 stoichiometry, and the single-crystal structure was solved and refined in the monoclinic system with the $C2/c$ space group and one DAP molecule and two SUL molecules in the asymmetric unit. Hydrogen bonding in the crystal structure of DAP·SUL is very complex. There are multiple potential H-bonding donors/acceptors in both DAP and SUL molecules. Each of these groups can participate in the formation of at least two hydrogen bonds. Major H-bonding interactions can be identified in the complementary sulfonamide−sulfonamide interactions of SUL to form a one-dimensional chain structure (Figure 3a). Specifically, the sulfonamide group of SUL was connected with the other two SUL molecules by intermolecular $N_5-H_{27}\cdots O_3$ (2.23 Å) and $N_5-H_{28}\cdots O_4$ (2.49 Å) hydrogen bonds to give a one-dimensional chain structure along the *a* axis. The amino group of DAP was also found to form a H-bonding interaction with the sulfonamide oxygen from SUL via synthon **I** ($N_6-H_{15}\cdots O_1$, 2.54 Å). The sulfonyl group of DAP, on the other hand, formed a H-bonding interaction with the aromatic amino group of SUL also via synthon **I** ($N_1-H_{4B}\cdots O_4$, 2.20 Å). The multiple H-bonding interactions between DAP and SUL result in the 3D packing pattern depicted in Figure 3b.

Interestingly, although different crystallization methods were employed, attempts to synthesize DAP co-crystals with other sulfanilamide derivatives, such as SD), SFM, or SFD, were unsuccessful (Table S2, Supporting Information). The sulfonamide−sulfonamide interactions were found to be a key factor in the formation of the DAP·SUL co-crystal. If one hydrogen atom on the amino group of the coformers is replaced with other bulky substitutions, the one-dimensional sulfonamide H-bonding chain structure cannot be formed due to the steric hindrance, and hence, the co-crystal structure cannot be built.

DAP·FLA Co-Crystal. Encouraged by the successful result for the DAP·SUL example, we then extended our studies to compounds containing a carbonyl moiety. DAP and FLA were crystallized in 1:1 stoichiometry. The crystal structure was solved and refined in the monoclinic system with the $P2_1/n$ space group and one DAP molecule and one FLA molecule in the asymmetric unit. As expected, the carbonyl groups of FLA formed H-bonding interactions with the amino groups of DAP to form a tetrameric aggregation as depicted in Figure 4a. Two host molecules and two guest molecules are linked by hydrogen bonding between the carbonyl and the amine groups via synthon **II** ($N_2-H_{10B}\cdots O_4$, 2.11 Å; $N_1-H_{4A}\cdots O_4$, 2.08 Å) to give a tetrameric structure. Along the *b* axis, the host molecules are also connected by hydrogen bonding via synthon **I** ($N_2-H_{10A}\cdots O_1$, 2.16 Å) to form a one-dimensional chain (Figure

dx.doi.org/10.1021/cg500668a | *Cryst. Growth Des.* 2014, 14, 4562−4573

4b). These chains are further linked by hydrogen bonding via synthon **II** depicted previously to form a two-dimensional network structure. As the amino group can serve as both a H-bonding donor and a H-bonding acceptor, the *bc* layers were further extended through $N_1-H_{4B}\cdots N_2$ (2.43 Å) hydrogen bonding along the *a* axis to generate its 3D structure (Figure 4c).

DAP·LUT Co-Crystal. The dapsone−luteolin co-crystal was crystallized in the monoclinic system with the $P2_1/c$ space group. The asymmetric unit contains one dapsone, one luteolin, and an ethanol molecule (Figure 5a). As LUT is also a

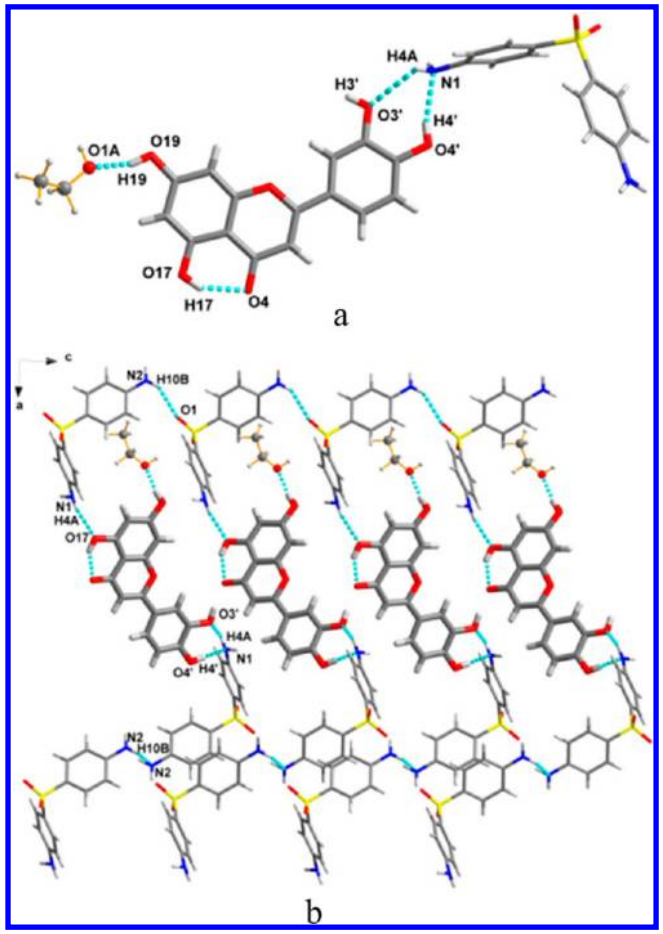

Figure 5. (a) Major crystal interactions. (b) 2D sheet running along the *b* axis of DAP·LUT.

flavonoid coformer, the crystal structure of DAP·LUT presents some similarities to that of the DAP·FLA co-crystal. The DAP host molecules are connected by an intermolecular H-bonding interaction between the amino group and sulfonyl oxygen via synthon **I** ($N_2-H_{10B}\cdots O_1$, 2.50 Å) to form one-dimensional chains along the *c* axis. Between the DAP chain structures, luteolin molecules also arrange in chains parallel to the DAP chain and form H-bonding interactions with the amino groups from DAP ($N_1-H_{4A}\cdots O_{17}$, 2.37 Å; $N_1-H_{4A}\cdots O_{3'}$, 2.16 Å; $O_{4'}-H_{4'}\cdots N_1$, 2.12 Å) to form a two-dimensional network structure (Figure 5b). Isolated ethanol molecules were found to fill into the void space and form H-bonding interactions with the phenol groups of LUT. It was found that the inclusion of ethanol molecules is important in facilitating the formation of the DAP·LUT co-crystal. When other solvents were utilized, no co-crystal of DAP·LUT could be obtained even with the same crystallization conditions. Interestingly, the inclusion of ethanol solvent was also found to be vital in stabilizing the co-crystal. When the co-crystal sample was subjected to thermal stress, ethanol molecules could be released at 170 °C under reduced pressure. However, the resulting solid was found to change back to a physical mixture of DAP and LUT after the ethanol molecules were removed from the crystal lattice (Figure S1, Supporting Information). Notably, attempts to grow DAP co-crystals with structural analogues of LUT, such as FIS and GEN, were unsuccessful under similar crystallization conditions (Table S2, Supporting Information). These findings further confirmed that two phenolic hydroxyl groups ($-O_{17}H_{17}$ and $-O_{3'}H_{3'}$) play important roles in construction of the unique H-bonding interactions between DAP and LUT molecules. When either of the phenol groups is absent, such as FIS and GEN, a co-crystal with DAP cannot be synthesized. The two hydroxyl groups perform a pivotal function in the formation of the two-dimension network in the DAP·SUL co-crystal.

DAP·CAF Co-Crystal. Depending on the crystallization solvent mixture utilized, DAP and CAF were found to crystallize in 1:1 and 1:2 stoichiometries to give DAP·CAF-1 and DAP·CAF-2 co-crystals, respectively. The crystal structure of DAP·CAF-1 was solved and refined in the orthorhombic system with the *Pbca* space group. One DAP molecule and one CAF molecule are included in the asymmetric unit. Notably, a cyclic tetramer structure constructed by four DAP molecules connected via consecutive H-bonding interactions via synthon **I** ($N_1-H_{4B}\cdots O_1$, 2.17 Å; $N_2-H_{10A}\cdots O_2$, 2.13 Å) (Figure 6a). Caffeine molecules were found to be anchored on the amino group of each DAP molecule via synthon **II** ($N_2-H_{10B}\cdots O_3$, 2.02 Å). These tetramers further extended into the 2D H-bonding network via synthon **I** along the *a*-axis and *b*-axis to form a grid-sheet structure (Figure 6b).

Compared with the crystal structure of DAP·CAF-1, that of the DAP·CAF-2 co-crystal presents obviously different unit cell parameters and a much more complex hydrogen-bonding network. DAP·CAF-2 was solved in the orthorhombic crystal system with the $Pna2_1$ space group and two DAP molecules and four CAF molecules in the asymmetric unit. The CAF molecules present both complex hydrogen-bonding formations and complex packing patterns. These CAF molecules can be divided into four types. Each type of CAF molecule shows different H-bonding and packing patterns via synthon **II** (Figure 7a). When viewed along the *c* axis, the DAP molecules and CAF molecules are constructed into two types of 2D sheet structures. In the type A layer, DAP molecules are intermolecularly H-bonded via synthon **I** ($N_1-H_{4B}\cdots O_2$, 2.49 Å), forming infinite chains of DAP. The CAF molecules are connected by nonclassic auxiliary C−H···O H-bonding interactions ($C_{220}-H_{68}\cdots O_{23}$, 2.36 Å) to generate chains of CAF molecules along the *a* axis. These chains interweave with each other via synthon **II** ($N_1-H_{4A}\cdots O_{24}$, 2.31 Å), forming a 2D network structure (Figure 7b). In the type B layer, zigzag CAF chains are connected via nonclassic hydrogen-bonding interactions ($C_{119}-H_{112}\cdots O_3$, 2.58 Å; $C_{20}-H_{20}\cdots O_{14}$, 2.41 Å). Between the 1D infinite chains, the CAF molecules are linked via synthon **II** ($N_2-H_{10A}\cdots O_{13}$, 2.17 Å; $N_2-H_{10B}\cdots O_4$, 2.13 Å) to give a 2D H-bonding network (Figure 7c). These two types of layers assemble in an "AAB" fashion along the *c* axis to construct the 3D structure of DAP·CAF-2 (Figure S2, Supporting Information).

Interestingly, each CAF molecule contains three N-substituted methyl groups in the structure. It was found that

dx.doi.org/10.1021/cg500668a | *Cryst. Growth Des.* 2014, 14, 4562−4573

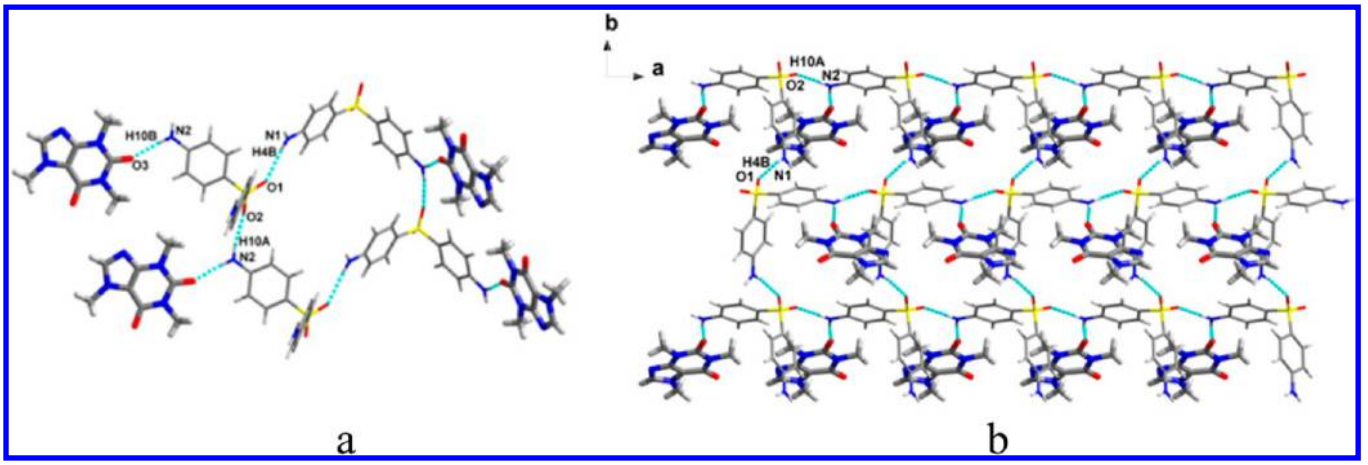

Figure 6. (a) Supramolecular tetramer unit of DAP·CAF-1. (b) 2D structure of DAP·CAF-1 viewed along the *c* axis.

the two methyl groups (designated as Me-A and Me-B) play crucial roles in the architecture of the corresponding crystal structures of the CAF co-crystals (Figure 8). Particularly, in the DAP·CAF-1 crystal structure, Me-A participates in the formation of a one-dimensional chain structure with DAP molecules via $C_{13}-H_{13A}\cdots N_6$ (2.72 Å) hydrogen bonding and Me-B forms a strong C−H···π interaction ($C_{19}-H_{19C}\cdots\pi$, 3.01 Å) with the DAP molecules (Figure 8a). In DAP·CAF-2, Me-A is connected with the host molecule via $C_{13}-H_{13A}\cdots O_{2'}$ (2.56 Å) hydrogen bonding and Me-B is connected to another CAF molecule via $C_{19}-H_{19B}\cdots O_{14}$ (2.36 Å) hydrogen bonding (Figure 8b). Noticeably, a DAP co-crystal could not be formed when analogues of CAF, such as THP and THB, were used under similar crystallization conditions (Table S2, Supporting Information).

DAP·HBZ Co-Crystal. The single-crystal structure of DAP·HBZ was solved and refined in the monoclinic system with the $P2_1/n$ space group. One DAP molecule and one HBZ molecule are included in its asymmetric unit. The DAP·HBZ co-crystal resembles an inclusion complex (Figure 9a). Four DAP molecules are combined by intermolecular hydrogen bonding between two amino groups ($N_1-H_{4A}\cdots N_2$, 2.33 Å) and H-bonding between the amino and sulfonyl groups via typical synthon **I** ($N_2-H_{10B}\cdots O_2$, 2.41 Å) to form tetrameric structures. These tetramers are extended via the $R_4^4(20)$ ring motif to form a two-dimensional network structure (Figure 9b). Two guest molecules are interconnected via homomeric synthon $R_2^2(8)$ to form a dimer, and such dimers are incorporated into the DAP tetramer cages. Nonclassic contacts, including $C_{14}-H_{14}\cdots\pi$ (2.60 Å), $C_{15}-H_{15}\cdots\pi$ (2.66 Å), $C_{16}-H_{16}\cdots O_2$ (2.64 Å), and $S_2\cdots\pi$ (3.55 Å), further stabilize the incorporation of guest HBZ into this structure (Figure 9c).

Powder X-ray Diffraction and FT-IR Spectroscopy. The XRPD patterns of the six co-crystals and the parent compound DAP are compared (Figure S3, Supporting Information). The results show that the XPRD patterns of the co-crystals are significantly different from that of DAP itself. All the experimental XRPD patterns of the bulk samples closely match the patterns simulated from the corresponding single-crystal diffraction data. The excellent agreement confirmed the high purity and homogeneity of the bulk co-crystals. Noticeably, the bulk solid of DAP·CAF-2 was found to be a mixture of DAP·CAF-1 and DAP·CAF-2. Surprisingly, attempts to prepare pure DAP·CAF-2 powder were unsuccessful even with a significant effort to change the crystallization method.

The sensitivity of mid-IR spectra to the solid-state form has rendered them a useful tool for characterization and study of co-crystal formation. The FT-IR spectra of DAP and its co-crystals are compared in Figure S4 (Supporting Information). Because of the changes in H-bonding patterns and interactions, significant differences were observed between the co-crystals and DAP in the vibration frequency corresponding to the aromatic amino moiety and sulfonyl groups ranging from 3300 to 3500 cm^{-1} and from 1100 to 1300 cm^{-1}, respectively.

Thermal Analysis. All the solids were analyzed by TGA and DSC to probe the thermal stability and purity. The decomposition temperature and melting point of each co-crystal along with the corresponding data for the pure components are summarized in Table 4. The results show that the decomposition temperatures of these co-crystals are correlated to their coformers. Generally speaking, the higher the thermal stability of the coformer, the higher the thermal stability of the corresponding co-crystal. The DSC thermograms of DAP·FLA, DAP·CAF-1, and DAP·HBZ present sharp endotherms for melting, confirming the bulk purity and homogeneity (Figures S5−S7, Supporting Information). The DSC curve of DAP·LUT presents a pronounced endothermic peak at 172 °C, corresponding to the liberation of ethanol molecules, and such an endotherm signal is also echoed in the weight loss step in the corresponding TGA diagram (Figure S8, Supporting Information). A phase transition was detected in the DSC ramp of the DAP·SUL co-crystal (Figure S9, Supporting Information). To study the thermodynamic property of DAP·SUL, hyper-DSC was employed to investigate the unstable polymorphic form transformation behavior under accelerated heating rates. The phase transformation can be almost fully inhibited when the scan rate reaches 150 °C/min or higher (Figure S10, Supporting Information).

Solubility and Dissolution. Equilibrium solubility was determined by slurrying an excess amount of materials under various buffer conditions, including pH 2.0, 4.6, 6.8 buffers and 1% Tween 80 aqueous solution. The residual solids were examined by XRPD, and the solubility results were compared with those of the pure DAP drug (Table 5; Figures S11−S16, Supporting Information). The solubility of DAP at pH 4.6 and 6.8 was determined to be 0.17 mg/mL, which agrees well with the results from the literature.[9] No significant solubility improvement was observed for all the co-crystals studied in 1% Tween 80 solution. However, DAP·CAF-1 exhibits about 1.8 times higher equilibrium solubility than the DAP pure form

dx.doi.org/10.1021/cg500668a | *Cryst. Growth Des.* 2014, 14, 4562−4573

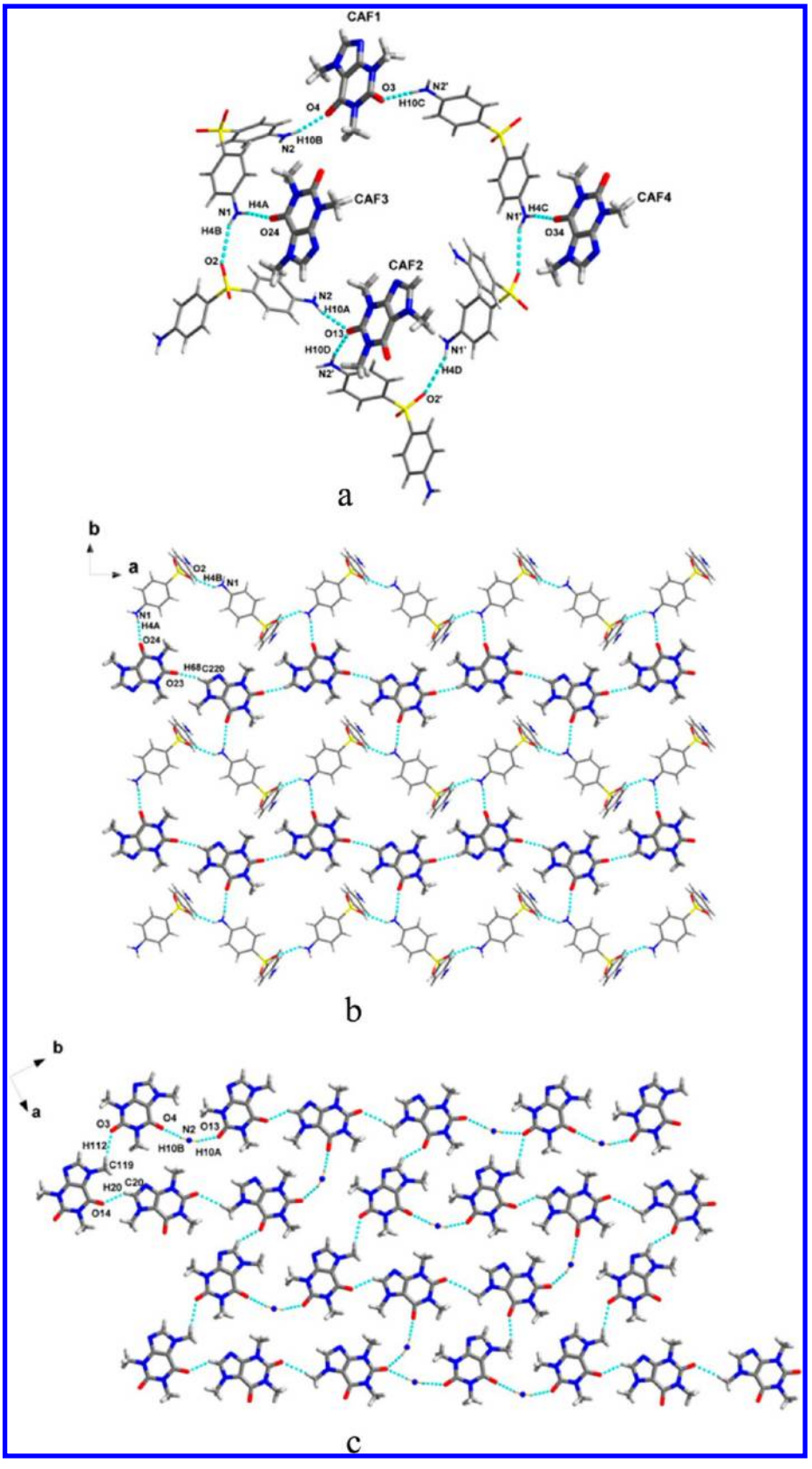

Figure 7. (a) Major interaction between the four types of CAF and host molecules in DAP·CAF-2. (b) Type A layer in DAP·CAF-2. (c) Type B layer in DAP·CAF-2. Only the amino groups are depicted for clarity.

in both pH 4.6 and pH 6.8 media. No solid form transformation was observed with DAP·SUL, DAP·CAF-1, and DAP·HBZ during the solubility experiments. However, for DAP, DAP·FLA, and DAP·LUT, solid-phase transformation was observed during the equilibrium process; consequently, the equilibrium solubility data cannot represent the true solubility

dx.doi.org/10.1021/cg500668a | *Cryst. Growth Des.* 2014, 14, 4562−4573

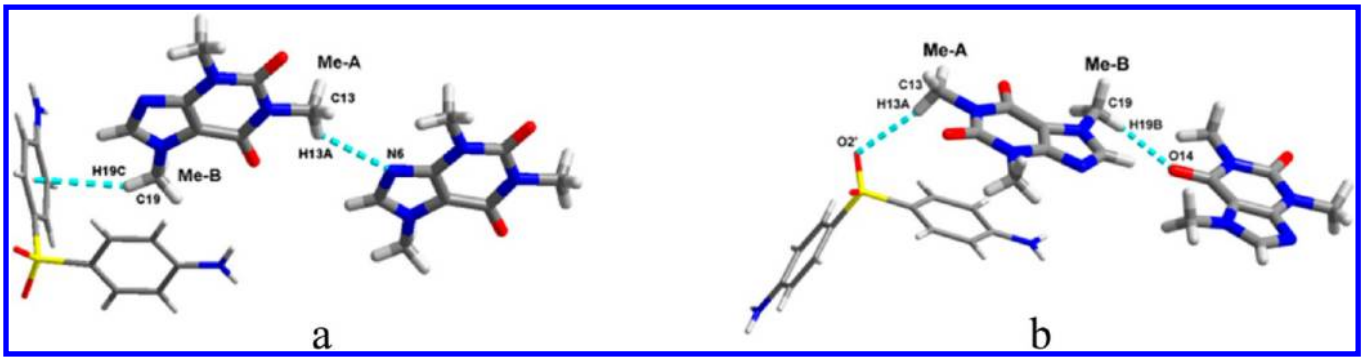

Figure 8. (a) Nonclassic contacts of the methyl groups in DAP·CAF-1. (b) Nonclassic contacts of the methyl groups in DAP·CAF-2.

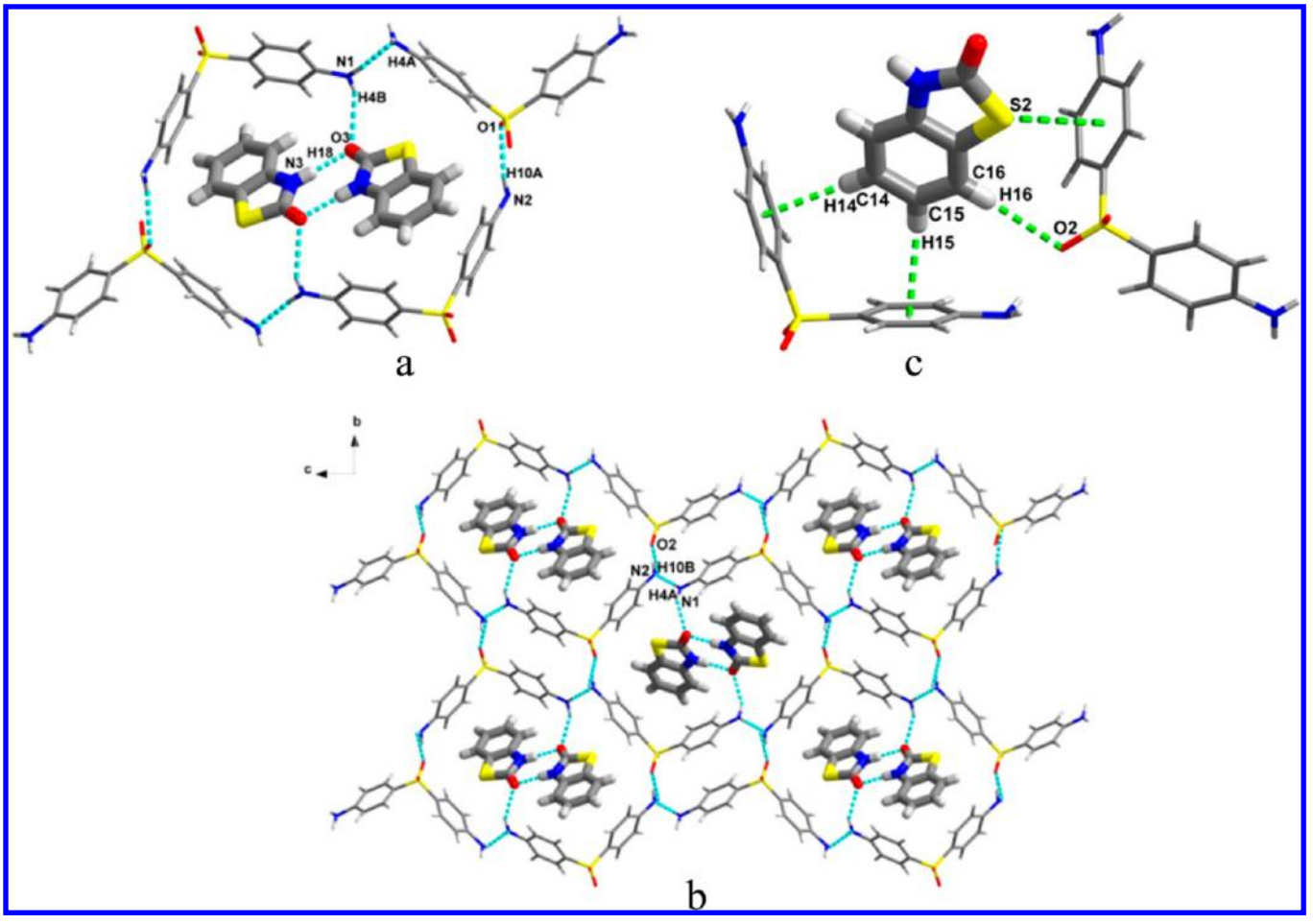

Figure 9. (a) Tetramer unit constructed by DAP and the attachment of the HBZ dimer to DAP. (b) 2D network of DAP·HBZ. (c) Nonclassic contacts for the stabilization of the coformer of DAP·HBZ.

Table 4. Decomposition Temperature and Melting Onset (°C) of DAP and Its Co-Crystals

compd	decomp temp (°C) of API/CCF	decomp temp (°C) of the co-crystal	mp (°C) of API/CCF	mp (°C) of the co-crystal
DAP·SUL	281/233	245	176/153	141
DAP·FLA	281/142	184	176/94	103
DAP·LUT	281/328	285	176/328	158
DAP·CAF-1	281/162 (sublimation)	162	176/–	172
DAP·HBZ	281/157	140	176/130	148

values of the corresponding starting materials. A close examination of the residual solids revealed that both DAP and the DAP·LUT co-crystal were converted to the DAP hydrate form and DAP·FLA was converted to a new co-crystal polymorph, which was characterized by NMR, XRPD, and thermal analysis (Figures S17−S20, Supporting Information). It is generally expected that when no phase transformation occurs, solubility is limited by both the lattice energy and solution energy (hydrophobicity of the solute). The melting point can be a critical parameter to access the lattice energy of the crystal. However, due to the involvement of different coformers in the solution, the solution energies cannot be directly compared. According to the solubility results, the inverse correlation

dx.doi.org/10.1021/cg500668a | *Cryst. Growth Des.* 2014, 14, 4562−4573

Table 5. Summary of the Equilibrium Solubility of DAP and Its Co-Crystals

material	apparent solubility ($mg \cdot mL^{-1}$) 1% Tween	pH 2.0	pH 4.6	pH 6.8	residue after equilibrium
DAP	0.85[a]	0.40[a]	0.17[a]	0.17[a]	DAP hydrate
DAP·SUL	0.92	0.38	0.19	0.18	co-crystal
DAP·FLA	0.92[a]	0.47[a]	0.20[a]	0.18[a]	new polymorph
DAP·LUT	0.26[a]	0.51[a]	0.20[a]	0.20[a]	DAP hydrate
DAP·CAF-1	0.81	0.65	0.30	0.31	co-crystal
DAP·HBZ	0.49	0.22	0.13	0.12	co-crystal

[a]The values correspond to the equilibrium solubility of the residue solids.

between the melting point and equilibrium solubility was not effectively observed in the DAP co-crystals.

The IDRs of DAP and its co-crystals were also studied under various buffer conditions (Table 6). The IDR trend of the co-crystals in 1% Tween is DAP·CAF-1 (66.2) > DAP·SUL (63.6) > DAP·HBZ (37.6) > DAP·FLA (24.6) > DAP·LUT (22.2), and this trend is directly correlated to the order of solubility of these co-crystals.

Table 6. Summary of Intrinsic Dissolution Rates of DAP and Its Co-Crystals

material	IDR ($\mu g \cdot cm^{-2} \cdot min^{-1}$) 1% Tween	pH 2.0	pH 4.6	pH 6.8
DAP	54.9	98.9	44.9	31.1
DAP·SUL	63.6	70.6	36.1	13.7
DAP·FLA	24.6	46.6	35.6	19.8
DAP·LUT	22.2	105.1	52.5	36.4
DAP·CAF-1	66.2	94.9	51.6	38.5
DAP·HBZ	37.6	52.4	12.1	18.8

Physical Stability. Pharmaceutical solids often contact water during the manufacturing and processing procedures, and they may also be exposed to humid air during storage. Hence, water may be absorbed to form new hydrate forms. Such transformation always results in products with drastically different physicochemical properties. Therefore, monitoring and controlling the physical stability is an important element during the course of whole drug development. Previous investigations have found that both DAP and caffeine can be converted to their corresponding hydrate forms when exposed to high relative humidity (RH), e.g., >75% RH or higher.[38,48] In this study, accelerated stability experiments were conducted to determine the physical stabilities of DAP and its co-crystals. The results show that DAP anhydrate was converted to its hydrate form when stored at 40 °C/75% RH for 4 months (Figure S21, Supporting Information) while the solid forms for all the co-crystals remained unchanged (Figures S22–S26, Supporting Information). Similar experiments were also performed using caffeine and its co-crystal DAP·CAF-1. After the materials were exposed to 98% RH for only 1 day at room temperature, caffeine was found to be converted to its hydrate form (Figure S27, Supporting Information) and the solid-state form of the DAP·CAF-1 co-crystal was found to remain unchanged. These results indicate that co-crystallization can be used as an important technique to improve the physical stability of particular drug substances.

CONCLUSIONS

As an alternative approach to improve the physicochemical and pharmacokinetic behaviors of drug substances, co-crystals arouse general interest in both academia and industry. Interest in the design and synthesis of co-crystals has explosively grown with an increasing number of publications on the subject in recent years. However, it is still a challenging task to precisely predict, rationally design, and successfully synthesize any co-crystal even with the simplest chemical structures. In this work, on the basis of an in-deep analysis of the characteristic crystal structure and functionalities of DAP, sulfonyl- and carbonyl-containing compounds were deliberately selected as coformers to prepare DAP co-crystals. The interactions between the aromatic amino groups of DAP and sulfonyl (synthon **I**) or carbonyl (synthon **II**) oxygen were utilized in designing and directing the synthesis of DAP co-crystals. Six drug–drug co-crystals of DAP were successfully prepared, and the structures were revealed by single-crystal X-ray diffraction analysis. Noticeably, in each series of structural analogues, not all coformers can successfully form co-crystals with DAP. Reoccurring packing patterns and H-bonding interactions via synthons **I** and **II** were observed in the various DAP co-crystals. The unsubstituted sulfonamide group in SUL was important in formation of the DAP·SUL co-crystal; the two unique phenol groups in DAP·LUT and the two indispensable methyl groups in DAP·CAF-1 and DAP·CAF-2 perform key roles in the architecture of the corresponding co-crystals. If such moieties of great importance are removed or replaced, the co-crystal structure cannot be built. In addition, the physicochemical properties of the DAP co-crystals were investigated by thermal analysis (TGA and DSC), PLM, XRPD, and Raman and FT-IR spectroscopy. Their equilibrium solubility and intrinsic dissolution rates were compared with those of the parent drug as well. The results show the influence of co-crystallization on the properties of DAP. This work also expands the pharmaceutically acceptable solid forms of DAP and supplements the successful cases of drug–drug co-crystals.

ASSOCIATED CONTENT

Supporting Information

Characterization data and crystallographic data files (CIF format). This material is available free of charge via the Internet at http://pubs.acs.org.

AUTHOR INFORMATION

Corresponding Author

*E-mail: xuefengmei@simm.ac.cn. Phone: 001-86-021-50800934.

Notes

The authors declare no competing financial interest.

ACKNOWLEDGMENTS

We thank the National Natural Science Foundation of China (Grant 81273479) and Chinese Academy of Science for funding.

REFERENCES

(1) Barr, J. *J. Hist. Med. Allied Sci.* **2011**, *66* (4), 425–467.
(2) Wozel, V. E. G. *Dermatol. Clin.* **2010**, *28* (3), 599–610.
(3) Lemmer, H.; Stieger, N.; Liebenberg, W.; Caira, M. R. *Cryst. Growth Des.* **2012**, *12* (3), 1683–1692.

(4) Martins, I.; Martins, M.; Fernandes, A.; Andre, V.; Duarte, M. T. *CrystEngComm* **2013**, *15* (40), 8173−8179.
(5) Grebogi, I. H.; Tibola, A.; Barison, A.; Grandizoli, C.; Ferraz, H. G.; Rodrigues, L. N. C. *J. Inclusion Phenom. Macrocyclic Chem.* **2012**, *73* (1−4), 467−474.
(6) Cao, X. H.; Gibbs, S. T.; Fang, L. Y.; Miller, H. A.; Landowski, C. P.; Shin, H. C.; Lennernas, H.; Zhong, Y. Q.; Amidon, G. L.; Yu, L. X.; Sun, D. X. *Pharm. Res.* **2006**, *23* (8), 1675−1686.
(7) Hughes, W. T. *Clin. Infect. Dis.* **1998**, *27* (1), 191−204.
(8) Monteiro, L. M.; Lione, V. F.; do Carmo, F. A.; do Amaral, L. H.; da Silva, J. H.; Nasciutti, L. E.; Rodrigues, C. R.; Castro, H. C.; de Sousa, V. P.; Cabral, L. M. *Int. J. Nanomed.* **2012**, *7*, 5175−5182.
(9) Calderini, A.; Martins, M. H.; Pessine, F. B. T. *J. Inclusion Phenom. Macrocyclic Chem.* **2013**, *75* (1−2), 77−86.
(10) Chougule, M.; Padhi, B.; Misra, A. *AAPS PharmSciTech* **2008**, *9* (1), 47−53.
(11) Pochopin, N. L.; Charman, W. N.; Stella, V. J. *Int. J. Pharm.* **1995**, *121* (2), 157−167.
(12) Smith, G.; Wermuth, U. D. *Acta Crystallogr., Sect. E: Struct. Rep. Online* **2012**, *68* (3), 669.
(13) Smith, G.; Wermuth, U. D. *J. Chem. Crystallogr.* **2013**, *43* (12), 664−670.
(14) Vishweshwar, P.; Nangia, A.; Lynch, V. M. *Cryst. Growth Des.* **2003**, *3* (5), 783−790.
(15) Trask, A. V.; Motherwell, W. D. S.; Jones, W. *Cryst. Growth Des.* **2005**, *5* (3), 1013−1021.
(16) Jones, W.; Motherwell, W.; Trask, A. V. *MRS Bull.* **2006**, *31* (11), 875−879.
(17) Bethune, S. J.; Schultheiss, N.; Henck, J. O. *Cryst. Growth Des.* **2011**, *11* (7), 2817−2823.
(18) Aher, S.; Dhumal, R.; Mahadik, K.; Ketolainen, J.; Paradkar, A. *Pharm. Dev. Technol.* **2013**, *18* (1), 55−60.
(19) Vangala, V. R.; Chow, P. S.; Tan, R. B. *CrystEngComm* **2011**, *13* (3), 759−762.
(20) Sanphui, P.; Goud, N. R.; Khandavilli, U. R.; Nangia, A. *Cryst. Growth Des.* **2011**, *11* (9), 4135−4145.
(21) Goud, N. R.; Gangavaram, S.; Suresh, K.; Pal, S.; Manjunatha, S. G.; Nambiar, S.; Nangia, A. *J. Pharm. Sci.* **2012**, *101* (2), 664−680.
(22) Hickey, M. B.; Peterson, M. L.; Scoppettuolo, L. A.; Morrisette, S. L.; Vetter, A.; Guzmán, H.; Remenar, J. F.; Zhang, Z.; Tawa, M. D.; Haley, S. *Eur. J. Pharm. Biopharm.* **2007**, *67* (1), 112−119.
(23) Thakuria, R.; Delori, A.; Jones, W.; Lipert, M. P.; Roy, L.; Rodríguez-Hornedo, N. *Int. J. Pharm.* **2013**, *453* (1), 101−125.
(24) Tao, Q.; Chen, J.-M.; Ma, L.; Lu, T.-B. *Cryst. Growth Des.* **2012**, *12* (6), 3144−3152.
(25) Shan, N.; Zaworotko, M. J. *Drug Discovery Today* **2008**, *13* (9), 440−446.
(26) Babu, N. J.; Nangia, A. *Cryst. Growth Des.* **2011**, *11* (7), 2662−2679.
(27) Good, D. J.; Rodríguez-Hornedo, N. *Cryst. Growth Des.* **2009**, *9* (5), 2252−2264.
(28) Bolla, G.; Sanphui, P.; Nangia, A. *Cryst. Growth Des.* **2013**, *13* (5), 1988−2003.
(29) Aitipamula, S.; Wong, A. B. H.; Chow, P. S.; Tan, R. B. H. *CrystEngComm* **2014**, *16*, 5793−5801.
(30) Sekhon, B. S. *Daru, J. Pharm. Sci.* **2012**, *20*, 45.
(31) Bhatt, P. M.; Azim, Y.; Thakur, T. S.; Desiraju, G. R. *Cryst. Growth Des.* **2008**, *9* (2), 951−957.
(32) Aitipamula, S.; Chow, P. S.; Tan, R. B. *CrystEngComm* **2009**, *11* (9), 1823−1827.
(33) Grobelny, P.; Mukherjee, A.; Desiraju, G. R. *CrystEngComm* **2011**, *13* (13), 4358−4364.
(34) Brittain, H. G.; Felice, P. V. US 8304404 B2, 2012.
(35) Veverka, M.; Simon, P.; Gallovic, J.; Jorik, V.; Veverkova, E.; Dubaj, T. *Monatsh. Chem.* **2012**, *143* (10), 1405−1415.
(36) Vitorino, G. P.; Sperandeo, N. R.; Caira, M. R.; Mazzieri, M. R. *Cryst. Growth Des.* **2013**, *13* (3), 1050−1058.
(37) Alleaume, M. Doctoral Thesis, University of Bordeaux, France, 1967.
(38) Yathirajan, H. S.; Nagaraja, P.; Nagaraj, B.; Bhaskar, B. L.; Lynch, D. E. Private communication, 2004.
(39) Hanafy, A.; Uno, J.; Mitani, H.; Kang, Y.; Mikami, Y. *Jpn. J. Med. Mycol.* **2007**, *48* (1), 47−50.
(40) Cushnie, T. P. T.; Lamb, A. J. *Int. J. Antimicrob. Agents* **2011**, *38* (2), 99−107.
(41) Sowa, M.; Ślepokura, K.; Matczak-Jon, E. *CrystEngComm* **2013**, *15* (38), 7696−7708.
(42) Cushnie, T. P. T.; Lamb, A. J. *Int. J. Antimicrob. Agents* **2005**, *26* (5), 343−356.
(43) Daly, J. *Cell. Mol. Life Sci.* **2007**, *64* (16), 2153−2169.
(44) Ucar, H.; Van derpoorten, K.; Cacciaguerra, S.; Spampinato, S.; Stables, J. P.; Depovere, P.; Isa, M.; Masereel, B.; Delarge, J.; Poupaert, J. H. *J. Med. Chem.* **1998**, *41* (7), 1138−1145.
(45) Roger, G.; Dollé, F.; De Bruin, B.; Liu, X.; Besret, L.; Bramoullé, Y.; Coulon, C.; Ottaviani, M.; Bottlaender, M.; Valette, H. *Bioorg. Med. Chem.* **2004**, *12* (12), 3229−3237.
(46) Foulon, C.; Duhal, N.; Lacroix-Callens, B.; Vaccher, C.; Bonte, J. P.; Goossens, J. F. *Eur. J. Pharm. Sci.* **2007**, *31* (3−4), 165−171.
(47) Sheldrick, G. M. *Acta Crystallogr., Sect. A: Found. Crystallogr.* **2007**, *64* (1), 112−122.
(48) Trask, A. V.; Motherwell, W. S.; Jones, W. *Cryst. Growth Des.* **2005**, *5* (3), 1013−1021.